Theory of Rayleigh-Bénard convection in planar nematic liquid crystals

Quanyuan Feng, Werner Pesch, and Lorenz Kramer
Physikalisches Institut der Universität Bayreuth, D-8580 Bayreuth, Germany
(Received 1 February 1991; revised manuscript received 3 September 1991)

A rigorous three-dimensional linear and weakly nonlinear analysis of Rayleigh-Bénard convection in planarly aligned nematic liquid crystals is presented. We use realistic boundary conditions and allow for a stabilizing magnetic field. The analysis includes a determination of all parameters of the amplitude equation in different regimes of the magnetic field where normal, oblique, and parallel rolls occur. It turns out that there exists a range at intermediate fields were the primary transition is subcritical for the standard material (4-methoxybenzylidene-4′-*n*-butylaniline). The ("nonlinear") stability of rolls is determined to second order in the amplitude so that nonpotential effects (especially mean flow) are included. In the low-field supercritical range the roll solutions are destabilized at a secondary threshold via a skewed-varicose instability leading presumably to spatiotemporal chaos. In the high-field supercritical normal-roll range a secondary transition can lead to oblique rolls that are ultimately destabilized by a short-wavelength instability.

PACS number(s): 47.25.Qv, 47.20.Ky, 61.30.Gd

I. INTRODUCTION

Rayleigh-Bénard convection (RBC) in isotropic fluid layers (pure fluids or mixtures) heated from below has been studied intensely during the past 25 years [1–3]. A characteristic feature of this system is its isotropy in the plane of the layer. As a consequence one may find periodic roll patterns, squares, or hexagons with arbitrary orientation at the convection threshold (we ignore the effects of boundaries). This holds as long as the patterns are stationary and the transition is continuous. Above but near threshold these patterns exist stably within wave-number bands that are limited by instabilities that reflect the symmetries: The Eckhaus instability, which is connected with translational invariance and is therefore very universal [4], and the zigzag instability, which is a consequence of rotational symmetry [1]. Additional instabilities come in at a finite distance from threshold (this is the case at least for the experimentally relevant rigid boundary conditions). As a result the ordered patterns may become unstable, resulting in a more or less disorganized dynamic state ("phase turbulence" or "weak turbulence" or "spatiotemporal chaos" [5]). In isotropic fluids this destabilization is affected by the skewed-varicose instability involving mean flow [6,7].

Clearly the study of pattern-forming instabilities in fluid layers with broken rotational symmetry is of interest, and here the use of liquid crystals is very helpful. Up to now much effort has been devoted to electrohydrodynamic convection (EHC) of planarly (homogeneously) aligned nematics [8–13]. This system has a strong axial anisotropy due to the surface anchoring of the director. As a consequence one can have at threshold normal rolls, which are aligned perpendicular to the undistorted director, or oblique rolls (roll axis oblique to the director), with interesting transitions between them. Starting from normal rolls at threshold one experimentally tends to find a secondary transition to oblique rolls, and then either a transition to a bimodal structure [8] or (probably more frequently) to spatiotemporal chaos [8,14,15]. There exists as yet no satisfactory quantitative explanation of these scenarios. Two reasons are responsible for this fact: First the usual theory is very complicated [13] and second it appears that additional mechanisms not contained in the standard description and not yet identified clearly play a role.

In this situation it seems important to study these phenomena in other pattern-forming systems with the same axial anisotropy, such as RBC in planarly aligned nematic liquid crystals. In this system the anisotropy of the thermal conductivity leads to spatial focusing of the heat current and thereby to a drastic lowering of the threshold compared to that of an isotropic fluid [16–18]. An advantage over EHC is the simpler structure of the standard hydrodynamic equations that are expected to quantitatively describe the experiments. In the past theoretical work on RBC in nematic liquid crystals has concentrated mostly on the two-dimensional linear stability analysis for normal rolls. The basic results agree well with the somewhat limited experimental observations [19]. Recently a full three-dimensional linear analysis has been done mainly with simplifying free boundary conditions [20,21]. It revealed that in some range of a stabilizing magnetic field oblique rolls occur at threshold, and transitions from normal to oblique and even parallel rolls (roll axis parallel to the director) are possible when the magnetic field is changed.

The nonlinear analysis of RBC in nematic liquid crystals has been carried out only to lowest order, i.e., $O(\epsilon^{1/2})$, where ϵ measures the distance from threshold in appropriate dimensionless units, to determine the nature of the bifurcation from the static to convective state. It has been confined to normal rolls and zero magnetic field. Utilizing free boundary conditions in Ref. [22], a supercritical (or forward) bifurcation for vanishing magnetic field was predicted. This result was subsequently

confirmed for rigid boundary conditions [23].

We here extend the weakly nonlinear analysis to arbitrary roll direction and arbitrary stabilizing magnetic fields. Moreover, we go to order ϵ (or more precisely, second order in the amplitude of the structure), so that nonpotential effects connected with mean flow are captured. From this analysis we can first decide whether the bifurcation at threshold is forward or backward. In our case we find in fact for the standard material 4-methoxybenzylidene-4-*n*-butylaniline (MBBA) a backward bifurcation at intermediate magnetic fields. Second, in the forward range, where our analysis yields the nonlinear roll solution near threshold, we can test its stability. We find that stable rolls are restricted to occur in a region of rather small ϵ, a situation which is reminiscent to the low-Prandtl-number case in isotropic fluids [1].

The paper is organized as follows. In Sec. II we describe the underlying thermohydrodynamic equations. Section III contains a full three-dimensional linear analysis with rigid boundary conditions. We present the threshold and the critical wave vector as functions of the magnetic field. We also provide an analytic approximation that captures the threshold behavior semiquantitatively. It is mainly used to gain some insight into the scenarios. In Sec. IV the weakly nonlinear analysis is introduced and applied to the periodic roll solutions. We give results for the amplitudes which can in principle be measured. In Sec. V the lowest-order amplitude equation that includes the slow modulations of the periodic pattern is presented and discussed. It describes destabilization of rolls by the two-dimensional Eckhaus mechanism. Section VI contains the higher-order weakly nonlinear analysis as applied to the stability of the rolls. We consider this the most important result of our work. In the low-field forward bifurcation range the destabilization for increasing ϵ is affected by a skewed-varicose mechanism where mean flow is decisive and which probably leads to spatiotemporal chaos. At high magnetic field the first destabilization of normal rolls is by the zig-zag (undulatory) mechanism, which can lead to a transition to oblique rolls. Section VII contains some concluding remarks. In Appendix A the dimensionless quantities used in this work and the full set of equations are given. Appendix B lists the material parameters for the material MBBA which are used for our calculations Similar results are available for 5CB (4-*n*-pentyl-4′-cyanobiphenyl) and can be obtained from the authors upon request. Details of the weakly nonlinear stability analysis of Sec. VI can be found in Appendix C.

II. FUNDAMENTAL EQUATIONS

The thermohydrodynamic equations for nematic liquid crystals, which involve the velocity field $\mathbf{v}$, temperature distribution T, and the director field $\mathbf{n}$, consist of the heat-transport equation, equations for the balance of momentum and angular momentum, and of the continuity equation together with constitutive relations. These equations are described in detail in Ref. [24], and will be collected here for convenience.

The heat-transport equation is

$$\frac{\partial T}{\partial t}+\mathbf{v}\cdot\nabla T=\kappa_\perp\nabla^2 T+\kappa_a\nabla\cdot[\mathbf{n}(\mathbf{n}\cdot\nabla T)]\ . \tag{2.1}$$

$\kappa_\parallel$ and $\kappa_\perp$ denote the thermal diffusivities parallel and perpendicular to the director axis, respectively. Temperature dependence of $\kappa_\parallel$ and $\kappa_\perp$ has been neglected. It is in particular the diffusivity anisotropy, $\kappa_a=\kappa_\parallel-\kappa_\perp$, that gives rise to the "heat-focusing mechanism" [16,17].

The equation for the director $\mathbf{n}$ can be interpreted as the balance of the total torque $\mathbf{\Gamma}$ exerted on the director. It has the form

$$\mathbf{n}\times\mathbf{\Gamma}=\mathbf{0}\ . \tag{2.2}$$

The torque $\mathbf{\Gamma}$ contains elastic, viscous, and in the presence of a magnetic field $\mathbf{H}$, magnetic contributions,

$$\mathbf{\Gamma}=-\frac{\delta G}{\delta\mathbf{n}}-\gamma_1\mathbf{N}-\gamma_2\mathbf{A}\cdot\mathbf{n}+\mu_0\chi_a(\mathbf{n}\cdot\mathbf{H})\mathbf{H}\ , \tag{2.3}$$

where γ_1 and γ_2 are the rotational viscosities which can be expressed in terms of the shear viscosities $\gamma_1=\alpha_3-\alpha_2$, $\gamma_2=\alpha_3+\alpha_2$. G is the elastic free-energy density

$$G=\tfrac{1}{2}[k_{11}(\nabla\cdot\mathbf{n})^2+k_{22}(\mathbf{n}\times\nabla\times\mathbf{n})^2+k_{33}(\mathbf{n}\times\nabla\times\mathbf{n})^2] \tag{2.4}$$

with the three elastic constants k_{11}, k_{22}, and k_{33}. The functional derivative $\delta G/\delta\mathbf{n}$ is defined as $\delta G/\delta n_i=\partial G/\partial n_i-\partial_j(\partial G/\partial n_{i,j})$ (the notations $\partial_j=\partial x_j$ and $n_{i,j}=\partial n_i/\partial x_j$ are used throughout). The viscous part is determined by the rate of change of the director relative to the moving fluid, $N=d\mathbf{n}/dt+\frac{1}{2}\mathbf{n}\times(\nabla\times\mathbf{v})$ ($d/dt=\partial_t+\mathbf{v}\cdot\nabla$, the substantial time derivative), and by the coupling of the symmetric strain tensor $\mathbf{A}$, i.e., $A_{ij}=\frac{1}{2}(v_{i,j}+v_{j,i})$, to the director.

From momentum conservation follows the equation of motion for the velocity field $\mathbf{v}$:

$$-\rho\frac{d\mathbf{v}}{dt}+\mathbf{F}+\nabla\cdot\mathbf{T}=\mathbf{0}\ , \tag{2.5}$$

where ρ is the mass density. $\mathbf{F}=\rho\mathbf{g}$ is the gravitational force ($\mathbf{g}$ is the gravitational acceleration) and $\mathbf{T}$ the stress tensor

$$T_{ij}=-p\delta_{ij}+s_{ij}+t_{ij}\ . \tag{2.6}$$

Apart from the pressure p the tensor is constructed from an elastic part

$$s_{ij}=-\frac{\partial G}{\partial n_{k,i}}n_{k,j}\ , \tag{2.7}$$

and the viscous stress tensor

$$\mathbf{t}=\alpha_1\mathbf{nn}(\mathbf{n}\cdot\mathbf{A}\cdot\mathbf{n})+\alpha_2\mathbf{nN}+\alpha_3\mathbf{Nn}+\alpha_4\mathbf{A}+\alpha_5\mathbf{n}(\mathbf{n}\cdot\mathbf{A})+\alpha_6(\mathbf{n}\cdot\mathbf{A})\mathbf{n} \tag{2.8}$$

with the viscosity coefficients α_i, $i=1,2,\ldots,6$. The quantity $\alpha_4/2$ corresponds to the isotropic viscosity.

The fluid will be treated as incompressible so that the continuity equation has the form

$$\nabla\cdot\mathbf{v}=0\ . \tag{2.9}$$

The usual experimental setup consists of a layer of a nematic liquid crystal of thickness d confined between two horizontal flat plates maintained at different temperatures. For convenience, we choose Cartesian coordinates (x,y,z) such that the lower and upper plates are situated at $z=-d/2$ and $d/2$, respectively. We concentrate on the planar configuration where the director at the upper and lower boundaries is parallel to the confining plates and aligned along the x axis. The applied magnetic field is also taken along that direction $[\mathbf{H}=(H,0,0)]$, so that it provides additional stabilization of the planar configuration.

As in the Boussinesq approximation, we neglect the temperature variation of material parameters across the slab with the exception of the mass density ρ in the gravitation force in Eq. (2.5)

$$\rho(T)=\rho_0[1-\alpha(T-T_0)] \tag{2.10}$$

(α is the thermal-expansion coefficient). Furthermore, the temperature distribution across the layer is described by its deviation ϕ from the undisturbed profile

$$T=T_0-\beta z+\phi(x,y,z,t) \tag{2.11}$$

with $\beta=(T_{z=-d/2}-T_{z=d/2})/d$ and T_0 the temperature in the middle plane without convection.

The general equations are always satisfied by the homogeneous solution $\phi=0$, $\mathbf{v}=\mathbf{0}$, $n_x=1$, $n_y=n_z=0$. The most natural variables to describe the convective state are therefore $\mathbf{v}$, n_z, n_y, and ϕ; n_x results from the normalization $\mathbf{n}^2=1$.

The assumed incompressibility of the fluid is taken into account by the introduction of two velocity potentials f and g [25]

$$\mathbf{v}=\boldsymbol{\delta} f+\boldsymbol{\epsilon} g \ , \tag{2.12}$$

where the differential operators $\boldsymbol{\delta}$ and $\boldsymbol{\epsilon}$ are defined as

$$\boldsymbol{\delta}=(\partial_x\partial_z,\partial_y\partial_z,-\partial_x^2-\partial_y^2), \quad \boldsymbol{\epsilon}=(\partial_y,-\partial_x,0). \tag{2.12'}$$

The application of these operators on Eq. (2.5) leads to two equations for f and g, in which the pressure is eliminated.

The torque-balance equation (2.2) determines only the torque components locally perpendicular to $\mathbf{n}$. We obtain the relevant two equations by projection of $\boldsymbol{\Gamma}$ on the corresponding local coordinate system

$$\boldsymbol{\Gamma}\cdot(\mathbf{n}\times\hat{\mathbf{z}})=0, \quad \boldsymbol{\Gamma}\cdot[\hat{\mathbf{z}}-\mathbf{n}\cdot(\hat{\mathbf{z}}\cdot\mathbf{n})]=0 \ , \tag{2.13}$$

with $\hat{\mathbf{z}}$ the unit vector in z direction.

Finally the equations are to be supplemented by the realistic rigid boundary conditions

$$\phi=n_z=n_y=f=\partial_z f=g=0 \quad \text{at } z=\pm d/2 \ . \tag{2.14}$$

Sometimes we shall also refer to results based on free boundary conditions

$$\phi=n_z=\partial_z n_y=f=\partial_z^2 f=\partial_z g=0 \quad \text{at } \mathbf{z}=\pm d/2 \ . \tag{2.15}$$

The whole system of equations is written in dimensionless form as explained in Appendix A. One is then left with three important dimensionless parameters that determine the physical properties: The Rayleigh number R as main control parameter, the Prandtl number P_r which is the ratio of the thermal and viscous diffusion times, and F, the ratio of the director-relaxation and the thermal diffusion times

$$R=\frac{\alpha g\rho_0\beta d^4}{(\alpha_4/2)\kappa_\perp}, \quad \mathrm{Pr}=\frac{\alpha_4/2}{\rho_0\kappa_\perp}, \quad F=\frac{\gamma_1 d^2/k_{11}}{d^2/\kappa_\perp}=\frac{\gamma_1\kappa_\perp}{k_{11}} \ . \tag{2.16}$$

An additional control parameter is supplied by the magnetic field which we choose parallel to the x axis so that it stabilizes the unperturbed state. We use the dimensionless field $\mathbf{h}=\mathbf{H}/H_f$, where

$$H_f=(\pi/d)[k_{11}/(\mu_0\chi_0)]^{1/2} \tag{2.17}$$

is the splay-Fréedericksz transition threshold.

In the following we will often use a shorthand notation for the five equations which determine the unknowns ϕ, n_z, n_y, f, and g. When these quantities are combined to a vector $\mathbf{V}$, the equations read symbolically

$$L\mathbf{V}+\mathbf{N}_2(\mathbf{V}|\mathbf{V})+\mathbf{N}_3(\mathbf{V}|\mathbf{V}|\mathbf{V})+\cdots =(B_0+B_1(\mathbf{V})+B_2(\mathbf{V}|\mathbf{V})+\cdots)\frac{\partial}{\partial t}\mathbf{V} \ . \tag{2.18}$$

The quantities L and B_i denote matrix differential operators. The components of vector $\mathbf{N}_2$ ($\mathbf{N}_3$) are quadratic (cubic) in $\mathbf{V}$ and its spatial derivatives. These quantities are obtained by a systematic expansion of our basic equations. The explicit expressions are somewhat lengthy and will not be reproduced in this paper.

III. LINEAR ANALYSIS

A. General formulation

With increasing control parameter R, the homogeneous state $\mathbf{V}=(\phi,n_y,n_z,f,g)=\mathbf{0}$ loses stability at a critical threshold value R_c. According to the standard technique one examines at first the general equations (2.18) linearized around $\mathbf{V}=\mathbf{0}$, i.e.,

$$L(\partial_x,\partial_y,\partial_z;R)\mathbf{V}-B_0(\partial_x,\partial_y,\partial_z)\frac{\partial}{\partial t}\mathbf{V}=\mathbf{0} \ , \tag{3.1}$$

and investigates the possibility of exponentially growing infinitesimal disturbances $\mathbf{V}$. Written out in detail Eq. (3.1) reads in dimensionless units (see Appendix A, the primes are left out)

$$(-\partial_t+\kappa_\parallel\partial_x^2+\partial_y^2+\partial_z^2)\phi-R\kappa_a\partial_x n_z-R\Delta_2 f=0 \ , \tag{3.2}$$

$$(\partial_z^2+k_{22}\partial_y^2+k_{33}\partial_x^2-F\partial_t-\pi^2h^2)n_z+(1-k_{22})\partial_y\partial_z n_y+\frac{F}{2}[-\nabla^2+\gamma(\Delta_2-\partial_z^2)]\partial_x f-\frac{F}{2}(1+\gamma)\partial_y\partial_z g=0 \ , \tag{3.3}$$

$$(k_{22}-1)\partial_y\partial_z n_z+(-\partial_y^2-k_{22}\partial_z^2-k_{33}\partial_x^2+F\partial_t+\pi^2h^2)n_y+F\gamma\partial_x\partial_y\partial_z f+\frac{F}{2}[\Delta_2-\gamma(\partial_x^2-\partial_y^2)]g=0\ , \tag{3.4}$$

$$-\Delta_2\phi+(\alpha_3\partial_z^2-\alpha_2\Delta_2)\partial_x\partial_t n_z+(\alpha_2+\alpha_3)\partial_x\partial_y\partial_z\partial_t n_y$$
$$+[\alpha_1\partial_x^4\partial_z^2+\tfrac{1}{2}(\alpha_5-\alpha_2)\partial_x^2\nabla^2\Delta_2+\nabla^4\Delta_2+\tfrac{1}{2}(\alpha_3+\alpha_6)\partial_x^2\partial_z^2\nabla^2-\nabla^2\Delta_2\partial_t/P_r]f+\partial_x\partial_y\partial_z[\alpha_1\partial_x^2+\tfrac{1}{2}(\alpha_3+\alpha_6)\nabla^2]g=0\ , \tag{3.5}$$

$$\alpha_3\partial_y\partial_z\partial_t n_z+(\alpha_3\partial_y^2-\alpha_2\partial_x^2)\partial_t n_y+[\alpha_1\partial_x^2+\tfrac{1}{2}(\alpha_3+\alpha_6)\nabla^2]\partial_x\partial_y\partial_z f$$
$$+[\alpha_1\partial_x^2\partial_y^2+\tfrac{1}{2}(\alpha_5-\alpha_2)\partial_x^2\Delta_2+\tfrac{1}{2}(\alpha_3+\alpha_6)\partial_y^2\nabla^2+\nabla^2\Delta_2-\Delta_2\partial_t/P_r]g=0\ , \tag{3.6}$$

where $\gamma=\gamma_2/\gamma_1$, $\nabla^2=\partial_x^2+\partial_y^2+\partial_z^2$, and $\Delta_2=\partial_x^2+\partial_y^2$.

The modal solutions for systems with a large aspect ratio (lateral dimension of the slab much larger than the thickness d) are of the general form $\mathbf{V}=\mathbf{V}_0(\mathbf{q},z)\exp(\lambda t+i\mathbf{q}\cdot\mathbf{x})$ with $\mathbf{q}=(q,p)$ and $\mathbf{x}=(x,y)$. Then in a shorthand notation Eqs. (3.2)–(3.6) transform into

$$[C(\mathbf{q},\partial_z)-RD(\mathbf{q},\partial_z)]\mathbf{V}_0=\lambda B_0(\mathbf{q},\partial_z)\mathbf{V}_0\ , \tag{3.7}$$

where L was decomposed into the R-independent operators C and D. One is then left with a system of coupled linear differential equations in z with the boundary conditions (2.14). Clearly the solution can be constructed by superposition of exponentials of z. The procedure is in practice often cumbersome because of numerical difficulties.

We have therefore solved the eigenvalue problem for λ by a Galerkin method. All quantities are expanded in terms of orthogonal functions of z which satisfy the boundary conditions Eq. (2.14). For the velocity potential f we have chosen the Chandrasekhar functions $C_n(z)$ [26,27]; for the remaining quantities (ϕ, n_z, n_y, and g) a set of trigonometric functions, namely $S_n(z)=\sin[n\pi(z+\frac{1}{2})]$, was used.

After truncation and projection onto the orthogonal set one is left with a homogeneous linear system for the expansion coefficients. The eigenvalues $\lambda(q,p;R,h)$ are determined by standard eigenvalue packages. Usually one needs only a few modes (not more than five for each quantity) and then the approach is very efficient. We have always checked our results by increasing the number of modes until deviations become insignificant.

For each eigenvector $\mathbf{V}_0$ of Eq. (3.7) one can construct a corresponding one $\mathbf{U}$ of an adjoint eigenvalue problem, defined by

$$L^+(\partial_x,\partial_y,\partial_z;R)\mathbf{U}=\lambda^* B_0^+(\partial_x,\partial_y,\partial_z)\mathbf{U}\ , \tag{3.8}$$

where the adjoint $\mathcal{O}^+$ of an operator $\mathcal{O}$ is defined as usual by the relation

$$\langle U,\mathcal{O}V\rangle=\langle\mathcal{O}^+\mathbf{U},\mathbf{V}\rangle \tag{3.9}$$

for arbitrary vectors $\mathbf{U}$ and $\mathbf{V}$ with

$$\langle\mathbf{U},\mathbf{V}\rangle=\int\mathbf{U}^{T*}\mathbf{V}\,d^3x \tag{3.10}$$

being the appropriate scalar product. The superscript T denotes the transposed vector. The integration is performed in an appropriate periodicity area in the x-y plane and across the width of the cell in the z direction. Note that $\langle\mathbf{U},L\mathbf{V}\rangle$ ($\langle\mathbf{U},B_0\mathbf{V}\rangle$) is zero if $\mathbf{U}$ and $\mathbf{V}$ do not belong to the same eigenvalue λ. The eigenvectors of the adjoint problem can also be classified by the wave vector $\mathbf{q}$ and expanded in terms of the same orthogonal function set C_n and S_n. In the framework of the truncated Galerkin expansion the adjoint problem is obtained from the transposed coefficient matrix of (3.7).

For fixed wave number $\mathbf{q}=(q,p)$ and small R all eigenvalues λ have negative real parts. We concentrate on the eigenvalue with the largest real part which is defined to be the *growth rate* $\sigma(q,p;R,h)$. When increasing the control parameter R the growth rate σ crosses zero from below and one has destabilization. From $\sigma(q,p;R,h)=0$ one gets the *neutral surface* $R_0=R_0(q,p)$. Minimizing R_0 with respect to (q,p) yields the *threshold* R_c and the *critical wave vector* $\mathbf{q}_c=(q_c,p_c)$. In our planar geometry we found that in all cases the imaginary part of λ is zero at the threshold. We have therefore always a steady bifurcation in contrast to a Hopf bifurcation as found in other cases (e.g., for homeotropic configuration [28,29]). For a steady bifurcation it is easier to determine R_c as the lowest positive eigenvalue of $(C-RD)\mathbf{V}_0=0$ instead of solving the general eigenvalue problem (3.7) for λ.

It turns out that the eigenvectors can be characterized by their symmetry under inversion of z. At the threshold the quantities ϕ, n_z, and f are symmetric (corresponding to S_n and C_n with odd n) while n_y and g are antisymmetric (S_n with even n).

The linear analysis also gives important information about the characteristic times and lengths. The growth rate σ can be expanded near threshold as follows:

$$\sigma=T_0^{-1}[R-R_0(\mathbf{q})]/R_c$$
$$=T_0^{-1}[\epsilon-\xi_1^2(q-q_c)^2-\xi_2^2(p-p_c)^2$$
$$-2a\xi_1\xi_2(q-q_c)(p-p_c)] \tag{3.11}$$

with $\epsilon=(R-R_c)/R_c$. The coherence lengths ξ_i and the parameter a, which is nonzero only for "oblique rolls" ($q_c\neq0$ and $p_c\neq0$, see below), are calculated from the relation

$$\langle\mathbf{U}(\mathbf{q}),L\mathbf{V}_0(\mathbf{q})\rangle=c_R[R-R_0(\mathbf{q})]/R_c\ , \tag{3.12}$$

valid near threshold with a proportionality factor c_R. $\mathbf{U}(\mathbf{q})$ denotes the adjoint eigenvector corresponding to the largest eigenvalue (the growth rate). The characteristic time T_0 is obtained from

$$T_0=\langle\mathbf{U}(\mathbf{q}_c),B_0\mathbf{V}_0(\mathbf{q}_c)\rangle/c_R\ . \tag{3.13}$$

Keeping the leading terms in the expansion of $R_0(\mathbf{q})$ around $\mathbf{q}_c$ leads directly to Eq. (3.11). The numerical results for T_0, ξ_1, ξ_2, and a will be given and discussed in Sec. V B.

B. Analytical threshold formula

The threshold behavior can be obtained semiquantitatively from the general linear equations by retaining only the leading mode in the Galerkin expansion. One then obtains a closed expression for the neutral surface $R_0(q,p)$ that can easily be evaluated on a pocket calculator [the primes for the dimensionless quantities (see Appendix A) are again left out]

$$R_0(q,p)=\frac{(\pi^2+\kappa_\parallel q^2+p^2)[\beta_2\beta_3-I_3^2(\beta_0-\beta_1)q^2p^2]^2}{I_1^2(q^2+p^2)^2[\beta_2+\pi^2\kappa_a FNq^2/(\gamma_1 M)]}\ , \tag{3.14}$$

where the following abbreviations have been used:

$$\beta_0=4\pi^2+\eta_1 q^2+p^2,\quad \beta_1=\eta_2(4\pi^2+p^2)+(-1+\alpha_1+\eta_1+\eta_2)q^2,\quad \beta_2=(\beta_0 q^2+\beta_1 p^2)\ ,$$
$$\beta_3=I_2(\eta_1 q^2+p^2)+I_5\{\alpha_1 q^4+[(\eta_1+\eta_2)q^2+2p^2](p^2+q^2)\}+2(\eta_1 q^2+p^2)(q^2+p^2)^2\ , \tag{3.15}$$
$$\eta_1=(2+\alpha_5-\alpha_2)/2,\quad \eta_2=(2+\alpha_3+\alpha_6)/2\ ,$$

$$N=K_1\left[-\alpha_2\beta_2/\pi^2+\alpha_3\beta_0+\alpha_3\left[1-\frac{I_3I_4}{\pi^2I_1}\right](\beta_1-\beta_0)\frac{p^2}{p^2+q^2}\right]-(1-k_{22})\frac{I_3I_4}{\pi^2I_1}(\alpha_2\beta_1+\alpha_3\beta_0)p^2\ ,$$

$$M=K_1K_2-(1-k_{22})I_4^2p^2\ , \tag{3.16}$$

$$K_1=4\pi^2k_{22}+k_{33}q^2+p^2+\pi^2h^2\ , \tag{3.17}$$
$$K_2=\pi^2+k_{33}q^2+k_{22}p^2+\pi^2h^2\ .$$

We have used the following overlap integrals (the integration runs from $-\frac{1}{2}$ to $\frac{1}{2}$ in our reduced units)

$$I_1=J\int dz\, C_1S_1,\quad I_2=J\int dz\, S_1\partial_z^4C_1\ ,$$
$$I_3=-J\int dz\, C_1\partial_zS_2,\quad I_4=-J\int dz\, S_1\partial_zS_2\ ,$$
$$I_5=-J\int dz\, C_1\partial_z^2C_1,\quad J^{-1}=\int dz\, S_1S_1=0.5\ ,$$

with the trigonometric functions $S_1(z)$, $S_2(z)$, and the Chandrasekhar function $C_1(z)$. The integrals have the following numerical values: $(I_1,I_2,I_3,I_4,I_5)=(1.3948, 2.6667, 4.9399, 24.6052, 1001.1278)$.

C. Results and discussion

In the following we present our results for the critical wave vector and the threshold. We have concentrated on accepted material parameters of MBBA (see Appendix B and Ref. [30]). In Fig. 1(a) the critical wave numbers are plotted as functions of the reduced magnetic field h. With increasing h the destabilizing modes at threshold (characterized by the wave vector $\mathbf{q}_c$) change their orientation in the x-y plane. First we have the rolls perpendicular to the x axis ("normal rolls," $q_c\neq0$, $p_c=0$) which is the conventional pattern. Then the roll pattern tilts ("oblique rolls," $q_c\neq0$, $p_c\neq0$), and finally the rolls are aligned parallel to the x axis ("parallel rolls," $q_c=0$, $p_c\neq0$). The transitions from normal rolls to oblique rolls (at $h\cong36$ in our units) and from oblique rolls to parallel rolls (at $h\cong62$) are continuous, that is, the wave vector $\mathbf{q}_c$ changes continuously. The two transition points, at which the symmetry of the roll pattern changes, will be called the lower ($h=36$) and upper ($h=62$) *Lifshitz points* as introduced in Ref. [8] for EHC and in analogy to the usage in the theory of phase transitions [31] (see also Sec. V A).

Figure 1(b) shows the threshold $R_c=R_0(q_c,p_c)$ as a function of the reduced magnetic field h. For not too large values of the field the threshold R_c behaves parabolically ($R_c=6.96+3.18h^2$); it increases then monotonically with the field and saturates at the values for isotropic fluids $R_c=1707.784$ with $q_c=0$, $p_c=3.117$ [27]. In this region the director distortion is suppressed altogether by the magnetic field and the remaining anisotropies of the viscosity play no role other than selecting the roll direction. Indeed Eqs. (3.2)–(3.6) reduce to the equations for an isotropic fluid with viscosity $\alpha_4/2$ and diffusivity $\kappa_\perp$ if one sets $n_z=n_y=0$ and $\partial_x=0$ [32]. Between the Lifshitz points the determination of R_c requires a three-dimensional calculation. For comparison we have included in Fig. 1(b) the results of a pure two-dimensional calculation where the rolls are forced to stay normal ($p=0$) for all values of h (upper dashed line). One obtains $q_c=2.16$ and $R_c=2060$ for $h\to\infty$, a value considerably higher than that for parallel rolls.

As far as normal rolls are concerned our results are consistent with the existing literature (for a recent review see [19]). The basic new instability mechanism through heat focusing was elucidated in a one-dimensional model [18] and needs no further explanation here. At zero magnetic field we can compare our results with those of Refs. [17, 30, 33–35] of a two-dimensional analysis. We get exactly the same threshold as that reported in Refs. [30] and [35], namely $q_c=3$, $\Delta T_c=2.7\,^\circ\mathrm{C}$. For finite magnetic fields agreement with the result of Ref. [35] is also found for normal rolls [i.e., the upper dashed curve in Fig. 1(b)].

The substantial difference from previous calculations

comes from the fact that for higher magnetic fields a three-dimensional calculation is necessary. This was noticed before in a calculation using free boundary conditions [20,21]. The main features of the bifurcation behavior were obtained there, but with considerable quantitative differences: The normal-oblique roll transition occurs at $h=17.5$ (instead of $h=36$ for rigid boundaries) and the oblique-parallel roll transition at $h=34.7$ (instead of $h=62$).

The characteristic features of the transition in the R-h plane are also obtained from the analytic approximation Eq. (3.14). In fact the threshold curve [Fig. 1(b)] changes by less than about 1% in comparison to the full numerical result. The two terms in the square bracket in the denominator characterize the two destabilization processes: The first term pertains to the classical isotropic mechanism, whereas the term proportional to κ_a describes the heat-focusing mechanism. Since F is usually large ($F=1182.65$ in our case) the heat focusing dominates except for high fields (then K_1 and K_2 become large and therefore N/M small). The heat-focusing mechanism usually favors normal rolls (note the factor q^2 in the expression) in contrast to the isotropic one which usually favors parallel ones, and this explains the rather complex threshold behavior. From Eq. (3.14) one sees that the anisotropy of the heat conductivity also enters into the first bracket in the numerator. This bracket is proportional to the heat diffusion [compare with Eq. (3.2)]. Now consider rolls with variable orientation and fixed spacing, so that q^2+p^2 is constant. Since $\kappa_\parallel > 1$ this contribution favors convection with $p\neq 0$ where heat diffusion is less efficient than for normal rolls ($p=0$) (note that horizontal diffusion counteracts convection). Thus by increasing $\kappa_\parallel$ one can in fact produce a situation with oblique rolls occurring at threshold at zero magnetic field. This tendency is aided by small values of k_{22} because this favors relief of splay by twist, which requires $p\neq 0$. Since this last effect is strongest at zero field [see $\mathbf{K}_2$ in Eq. (3.14)], the oblique rolls typically first vanish with increasing field and then reappear again at higher fields.

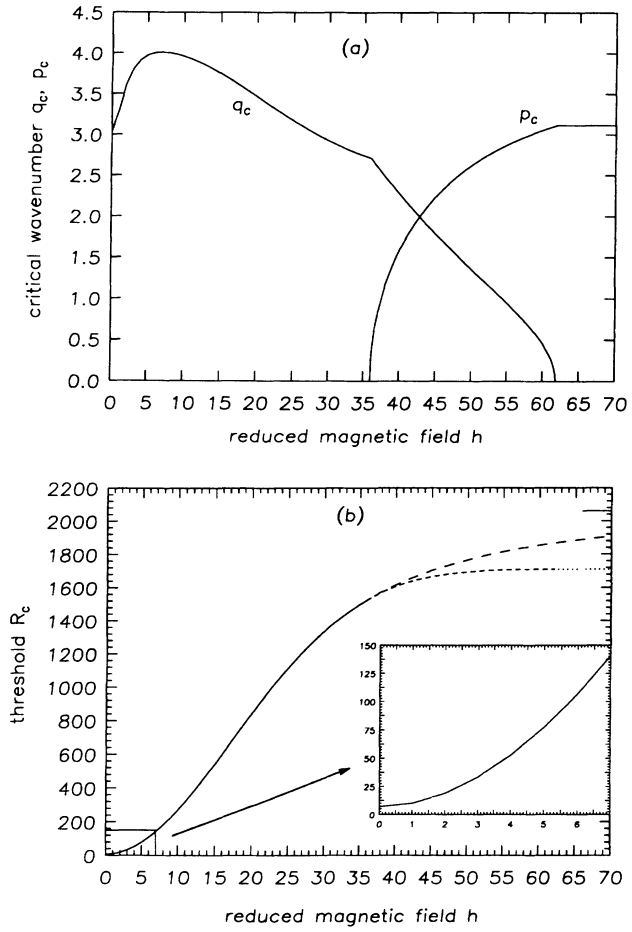

FIG. 1. (a) Critical wave numbers q_c and p_c as functions of the reduced magnetic field h ($H=hH_f$). For large h the critical wave number (and threshold) of the isotropic RBC is approaches with roll axis parallel to the director. (b) Threshold R_c as a function of h (solid line, normal rolls; dashed line, oblique rolls; dotted line, parallel rolls). The upper dashed line for higher magnetic fields results from a two-dimensional calculation (normal rolls), and the bar (above the upper dashed line) marks the asymptotic value $R_c=2060$ for $h\to\infty$.

Oblique rolls were observed at $h=0$ in an experiment [21]. A direct comparison with our results is not possible, because the confining plates in the experiment had rather poor heat conduction. In that case one would have to use different boundary conditions which have been shown to favor oblique rolls [21].

IV. PERIODIC ROLL SOLUTIONS IN A WEAKLY NONLINEAR ANALYSIS

A. General formulation

The treatment in this section will be initially kept general so that it applies also to later sections. From the linear analysis we obtain the destabilizing modes of the homogeneous rest state nucleating a roll pattern with wave number $\mathbf{q}$. Their growth rate σ vanishes at the neutral surface $R_0(\mathbf{q})$. For values of R slightly above the neutral surface, the absolute value of σ is small. The starting point of our perturbative expansion scheme will be a state that lies in the subspace spanned by the linear modes with small $|\sigma|$. The procedure corresponds to the center-manifold reduction for finite-dimensional dynamical systems [36]. Although for systems with an infinite number of degrees of freedom a mathematically rigorous justification is lacking, the approach is considered well founded from general principles [37–40]. It generalizes the well-known multiple time- and space-scale treatment of pattern-forming systems by the amplitude (or envelope) equation formalism [41] and now includes automatically higher-order derivatives and nonlocal contributions.

Thus the general solution is written up to second order in the amplitude in the form

$$\mathbf{V}=\mathbf{V}_1+\mathbf{V}_2\ , \tag{4.1}$$

where $\mathbf{V}_2$ is orthogonal to $\mathbf{V}_1$. The first part $\mathbf{V}_1$ represents a superposition of the linear modes $\mathbf{V}_0(\mathbf{q})$,

which depend on z and have been determined by the linear analysis [see Eq. (3.7)],

$$\mathbf{V}_1=\int d\mathbf{q}\, A(\mathbf{q},t)\exp(i\mathbf{qx})\mathbf{V}_0(\mathbf{q}) , \tag{4.2}$$

where the $\mathbf{q}$ integration extends at most over small regions centered around wave numbers $\pm\mathbf{q}_0$, where for given R the value of $\mathbf{q}_0$ is restricted by the condition $|[R-R_0(\mathbf{q}_0)]/R_0(\mathbf{q}_0)|\ll 1$. Since $\mathbf{V}_0(-\mathbf{q})=\mathbf{V}_0^*(\mathbf{q})$, the amplitude $A(\mathbf{q},t)$, which is yet undetermined, also satisfies $A(-\mathbf{q},t)=A^*(\mathbf{q},t)$ to ensure the reality of $\mathbf{V}_1$. Then making use of the fact that the amplitude $A(\mathbf{q},t)$ is small, we expand the nonlinearities of the general equations (2.18) systematically in powers of A up to the third order. $\mathbf{V}_2$ is evaluated in second order and finally $A(\mathbf{q})$ is determined from the third-order terms.

In general one would obtain nonlinear integro-differential equations for the amplitudes $A(\mathbf{q})$. If one is interested in periodic solutions the equations simplify considerably and one then obtains the conventional stationary-roll solutions. For wave vector $\mathbf{q}_0$ and R slightly above threshold, one starts with the following ansatz for the amplitude in (4.2):

$$A_r(\mathbf{q})=s(\mathbf{q}_0)\delta(\mathbf{q}-\mathbf{q}_0)+s^*(\mathbf{q}_0)\delta(\mathbf{q}+\mathbf{q}_0) , \tag{4.3a}$$

which corresponds to a stationary-roll solution

$$\mathbf{V}_{1r}=s(\mathbf{q}_0)\mathbf{V}_0(\mathbf{q}_0)\exp(i\mathbf{q}_0\cdot\mathbf{x})+\text{c.c.} \tag{4.3b}$$

$\mathbf{V}_{2r}$ is obtained from Eq. (2.18) at order A^2

$$L\mathbf{V}_{2r}+\mathbf{N}_2(\mathbf{V}_{1r}|\mathbf{V}_{1r})=0 . \tag{4.4a}$$

This equation can be treated with respect to the horizontal coordinates in Fourier space. The solution splits into three disjoint pieces of $\mathbf{V}_{2r}(\mathbf{q})$ with $\mathbf{q}=\pm 2\mathbf{q}_0$ and $\mathbf{q}=0$. For example, for $\mathbf{q}=2\mathbf{q}_0$ and $\mathbf{q}=0$, Eq. (4.4a) becomes

$$L(2\mathbf{q}_0)\mathbf{V}_{2r}(2\mathbf{q}_0)+s^2(\mathbf{q}_0)\mathbf{N}_2[\mathbf{V}_0(\mathbf{q}_0)|\mathbf{V}_0(\mathbf{q}_0)]=0 , \tag{4.4b}$$

$$L(0)\mathbf{V}_{2r}(0)+|s(\mathbf{q}_0)|^2\{\mathbf{N}_2[\mathbf{V}_0(\mathbf{q}_0)|\mathbf{V}_0(-\mathbf{q}_0)]+\mathbf{N}_2[\mathbf{V}_0(-\mathbf{q}_0)|\mathbf{V}_0(\mathbf{q}_0)]\}=0 . \tag{4.4c}$$

In (4.4b) and (4.4c) all derivative operators ∂_x and ∂_y have to be replaced by iq and ip, respectively, with appropriate wave vectors $\mathbf{q}$ [e.g., $2\mathbf{q}_0$ in the linear operator L in Eq. (4.4b)]. In a similar way we will in the following switch between real space and $\mathbf{q}$ space without always mentioning it explicitly. The z dependence of $\mathbf{V}_{2r}$ is treated by the same Galerkin ansatz as in the linear case. Equation (4.4a) therefore becomes a linear inhomogeneous system for the expansion coefficients of $\mathbf{V}_{2r}$, which can be solved uniquely because the inhomogeneity is orthogonal to the linear solutions (opposite symmetry with respect to the inversion of z).

At order A^3 we obtain from Eq. (2.18)

$$L\mathbf{V}_{1r}+\mathbf{N}_3(\mathbf{V}_{1r}|\mathbf{V}_{1r}|\mathbf{V}_{1r})+\mathbf{N}_2(\mathbf{V}_{2r}|\mathbf{V}_{1r})+\mathbf{N}_2(\mathbf{V}_{1r}|\mathbf{V}_{2r})=0 . \tag{4.5}$$

The first term in Eq. (4.5) is of order $[R-R_0(\mathbf{q}_0)]A_r$ which balances, as usual, the $O(A_r^3)$ terms. The amplitude is obtained by projecting (4.5) onto $\mathbf{V}_0$. Technically one switches again to $\mathbf{q}$ space and performs the scalar product [see Eq. (3.10)] with the adjoint eigenvector $\mathbf{U}(\mathbf{q})$ of the linear system. One gets an equation for $|s(\mathbf{q}_0)|^2$ of the following form:

$$|s(\mathbf{q}_0)|^2=-\frac{c_2(\mathbf{q}_0)}{c_3(\mathbf{q}_0)}\propto[R-R_0(\mathbf{q}_0)] \tag{4.6}$$

with the abbreviations

$$c_2(\mathbf{q})=\langle\mathbf{U}(\mathbf{q}),L(\mathbf{q})\mathbf{V}_0(\mathbf{q})\rangle , \tag{4.7a}$$

$$c_3(\mathbf{q})=d_2(\mathbf{q})+d_3(\mathbf{q}) , \tag{4.7b}$$

$$d_3(\mathbf{q})=c_3(-\mathbf{q},\mathbf{q},\mathbf{q})+c(\mathbf{q},\mathbf{q},-\mathbf{q})+c_3(\mathbf{q},-\mathbf{q},\mathbf{q}) , \tag{4.8}$$

$$c_3(\mathbf{q},\mathbf{q}_1,\mathbf{q}_2)=\langle\mathbf{U}(\mathbf{q}),\mathbf{N}_3[\mathbf{V}_0(\mathbf{q}_1)|\mathbf{V}_0(\mathbf{q}_2)|V_0(\mathbf{q}-\mathbf{q}_1-\mathbf{q}_2)]\rangle , \tag{4.9}$$

$$d_2(\mathbf{q})=\langle U(\mathbf{q}),\mathbf{N}_2[\bar{\mathbf{V}}_{2r}(0)|V_0(\mathbf{q})]+\mathbf{N}_2[\mathbf{V}_0(\mathbf{q})|\bar{\mathbf{V}}_{2r}(0)]\rangle+\langle U(\mathbf{q}),\mathbf{N}_2[\bar{\mathbf{V}}_{2r}(2\mathbf{q})|\mathbf{V}_0(-\mathbf{q})]+\mathbf{N}_2[\mathbf{V}_0(-\mathbf{q})|\bar{\mathbf{V}}_{2r}(2\mathbf{q})]\rangle , \tag{4.10}$$

where $\bar{\mathbf{V}}_{2r}(2\mathbf{q})\equiv\mathbf{V}_{2r}(2\mathbf{q})/s^2(\mathbf{q})$ and $\bar{\mathbf{V}}_{2r}(0)\equiv\mathbf{V}_{2r}(0)/|s(\mathbf{q})|^2$ [see (4.4a)].

The quantity c_2 is positive within the neutral surface. If c_3 is negative one has a forward or supercritical bifurcation. In Sec. IV B, it will be seen that one typically has a backward bifurcation ($c_3>0$) in an intermediate magnetic-field range. Then at least a quintic term in the amplitude $A(\mathbf{q})$ would be necessary for the description of the nonlinear regime. For $\mathbf{q}=\mathbf{q}_c$ ("band center") the amplitudes calculated here are to leading order proportional to $\epsilon^{1/2}$ with $\epsilon=(R-R_c)/R_c$.

In the practical calculation only a finite number ($=m_{oz}$) of z modes is retained. Following Busse [42], we consider the spatially averaged convective heat transport at the lower plate,

$$J_{\text{conv}}=-\overline{\partial_z\phi_s}|_{z=-1/2} \tag{4.11}$$

as a quantitative measure (which is also accessible experimentally). Changing the truncation number ($=m_{oz}$), we stop when the following criterion is satisfied:

$$|J_{\rm conv}(m_{oz}+2)-J_{\rm conv}(m_{oz})|/J_{\rm conv}(m_{oz})\leq 0.1\% \ .$$

It turns out that four z modes ($m_{oz}=4$) are sufficient for all practical purposes.

A more serious problem is the estimate of the range of validity of the amplitude expansion. This can in principle only be judged from a calculation including the quintic terms in the amplitude. For simplicity we consider the deviation of the director from the planar orientation in the midplane of the cell where it is maximal, and then $|n_z|<0.5$ as a rough estimate for the range of the validity. We found that the expansion should be applicable with semiquantitative results at least up to $\epsilon=0.1$ in all cases.

B. Results and discussion

We present some experimentally measurable quantities calculated from the nonlinear roll solution. In Fig. 2(a) the amplitudes (without the factor $\epsilon^{1/2}$!) at $\mathbf{q}_c$ of the z component of the director in the middle of the cell N_z and the y component N_y at $z=d/4$ are plotted as functions of h [i.e., one has $n_z(z=0)=\epsilon^{1/2}N_z\cos(\mathbf{q}\cdot\mathbf{x})$ and $n_y(z=d/4)=\epsilon^{1/2}N_y\sin(\mathbf{q}\cdot\mathbf{x})$]. In Fig. 2(b) we have plotted in a similar manner the quantity $(\mathrm{Nu}-1)/\epsilon$, where Nu is the Nusselt number, i.e., the spatially averaged total-heat current normalized to the conductive-heat current. The most important result is that N_z^2 and $(\mathrm{Nu}-1)/\epsilon$ turn out to be negative in the range $4.15<h<31$, indicating a backward bifurcation in that range. The quantity c_3 [Eq. (4.7b)] changes sign when one crosses the tricritical points $h=4.15$ and $h=31$, which results in the singular behaviors of N_z^2, N_y^2, and $(\mathrm{Nu}-1)/\epsilon$ at these points. Thus higher-order terms in the amplitude are needed to describe correctly nonlinear behaviors near the tricritical points and in the subcritical region.

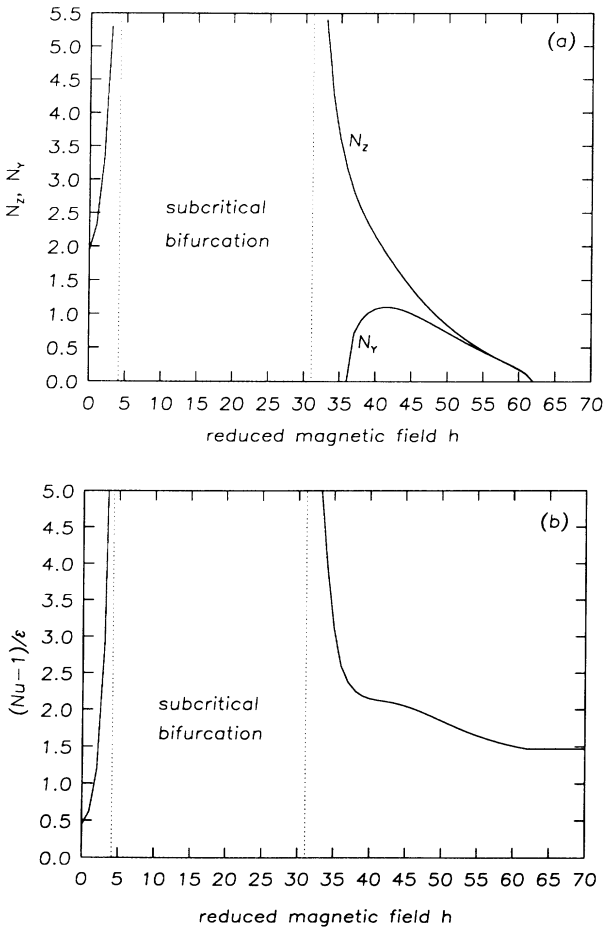

FIG. 2. (a) Amplitudes N_z and N_y of director components n_z and n_y (see text) at $\mathbf{q}=\mathbf{q}_c$ as functions of the reduced magnetic field h. (b) Reduced convective-heat transfer $(\mathrm{Nu}-1)/\epsilon$ (Nu is the Nusselt number) at $\mathbf{q}=\mathbf{q}_c$ as function of H.

A subcritical bifurcation has been found before in RBC with homeotropic configuration [29,43]. Although a simple and detailed physical explanation is lacking in both cases, the tendency can be understood by the following argument: The restoring torques are linear in n_z, i.e., harmonic for n_z near zero. The anharmonicity due to the magnetic field reduces the restoring forces (equal to negative anharmonicity, $\simeq -n_z^3$) as is characteristic for a dipole in an external field. The elastic restoring forces, on the other hand, have a positive anharmonicity for conventional materials with $k_{33}/k_{11}>1$. Increasing the magnetic field thus reduces the anharmonic contribution and therefore drives the system towards a backward bifurcation. For large fields the anharmonicities of the viscous forces become dominant, which again leads to forward bifurcation as in RBC for isotropic fluids.

V. AMPLITUDE EQUATION

A. General formulation

In Sec. IV we have constructed periodic roll solutions near threshold. One would like to describe more complicated situations such as modulations with respect to orientation and spacing of the rolls, point defects, and grain boundaries, and last but not least the stability of the roll pattern. It is well known that this can be achieved for long-wavelength modulations of the roll pattern at lowest order $O(\epsilon^{1/2})$ in the framework of the amplitude-equation formalism. One starts with a wave-packet solution where $A(\mathbf{q})$ is actually smeared out as provided for in Eq. (4.2). From $A(\mathbf{q})$ the conventional slowly varying amplitude (or envelope) $A(\mathbf{x})$, which appears in the amplitude equation, can be constructed by Fourier transformation. One then has

$$A(\mathbf{x},t)=\int d\Delta\mathbf{q}\,A(\mathbf{q}_c+\Delta\mathbf{q},t)\exp(i\Delta\mathbf{q}\cdot\mathbf{x}) \ . \qquad (5.1)$$

Typically the $\Delta\mathbf{q}$ integration is confined to a region $O(\epsilon^{1/2})$ and then $A(\mathbf{x})$ varies on a scale $\epsilon^{-1/2}$. It is evident that within the framework of the amplitude equation the quantity $c_2(\mathbf{q})$ in (4.7a) expanded around $\mathbf{q}_c$ to lowest order corresponds to the differential operator in the linear part, whereas $c_3(\mathbf{q})$ at $\mathbf{q}_c$ leads to the prefactor of the cubic term. Written out in detail we have

$$T_0\partial_t A(\mathbf{x},t)=(\epsilon+\xi_1^2\partial_x^2+\xi_2^2\partial_y^2+2a\xi_1\xi_2\partial_x\partial_y)A - g|A|^2A \ . \quad (5.2)$$

The determination of the characteristic time T_0, the lengths ξ_i, and the parameter a from the linear growth rate $\sigma(q,p;R)$ was already discussed in Sec. III A [note that the expression in Eq. (3.12) corresponds to $c_2(\mathbf{q})$, see also Eq. (4.7a)].

The coefficient of the cubic term is given by $g=-c_3(\mathbf{q}_c)/c_R$ with c_R defined in Eq. (3.12). One has $g>0$ for a forward bifurcation and $g<0$ for a backward bifurcation. The numerical value of g depends on the particular normalization chosen for the linear eigenvector of Eq. (3.7) and has no direct significance. We therefore preferred to give directly the amplitudes of the physical quantities as was done in Sec. IV B. All information can then be extracted from the amplitude equation. In fact, g can always be scaled to ±1. For $g>0$ roll solutions with wave vector $\mathbf{q}_0=\mathbf{q}_c+\mathbf{q}'$ correspond to periodic solutions of the amplitude equation $A(x)=A(q')\exp(i\mathbf{q}'x)$ with

$$|A(\mathbf{q}')|^2=(\epsilon-\xi_1^2q'^2-\xi_2^2p'^2-2a\xi_1\xi_2q'p')/g \ . \quad (5.3)$$

Clearly the solution exists inside a paraboloid which coincides to lowest order with the neutral surface. $A(\mathbf{q}')$ is then identical to $s(\mathbf{q}_0)$ in leading order $\epsilon^{1/2}$; see Sec. IV A, Eq. (4.6). If one scales down the paraboloid by a factor $(\frac{1}{3})^{1/2}$ one gets the stability region in $\mathbf{q}$ space. That is nothing else but the Eckhaus instability generalized to the two-dimensional case [31]. For normal (or parallel) rolls this reduces to the usual longitudinal Eckhaus instability. For isotropic systems one would in addition have the zigzag (or undulatory) instability which in the lowest-order amplitude-equation approximation renders all rolls with $q<q_c$ unstable. The zigzag instability occurs also in anisotropic systems at and near a Lifshitz point. Since there either ξ_2 or ξ_1 vanish (see below) a more complicated kind of amplitude equation with higher-order derivatives has to be used [31]. In that equation one also has locally stable undulated roll solutions (normal, oblique, or parallel) [44]. Within the simple amplitude equation (5.2) the only stable solutions in an infinite system are the straight rolls within the stable wave-vector range and there can be no transition to spatiotemporal chaos.

Carrying the expansion of $R_0(\mathbf{q})$ around $\mathbf{q}_c$ to higher order and transforming back to real space yields additional derivatives in the amplitude equation, which correspond to higher orders in ϵ. Such terms are, among others, responsible for corrections to the parabolic approximation of the neutral curve.

B. Results and discussion

In Fig. 3(a) the relaxation time T_0 in units of the vertical heat-diffusion time $d^2/\kappa_\perp$ is shown as a function of the reduced magnetic field. Similarly, in Fig. 3(b) the coherence lengths ξ_1 and ξ_2 in units of d, as well as the cross coefficient a in the oblique-roll range, are given for MBBA (see Appendix B for the material parameters used). The most obvious feature is the steep decrease of T_0 [$T_0\simeq47.13/(1+0.697h^2)$] for small fields by almost three orders of magnitude with increasing magnetic field. This reflects the fact that at zero field the director relaxation time $\tau_d\simeq\gamma_1d^2/k_{11}$ is by far the longest response time of the system and thus controls T_0. Clearly τ_d decreases with increasing field and eventually the heat-diffusion time becomes dominant. The strong dependence of the director relaxation time on the magnetic field h in nematics has obtain been stressed in the literature [19].

From Fig. 3(b) one sees that ξ_2 vanishes, like in EHC [11], at the lower Lifshitz point ($h\simeq36$), while ξ_1 vanishes at the upper one ($h\simeq62$). Whereas in EHC the parameter a is fairly small [11], it is near its maximally possible value 1 here (for $a>1$ the growth rate σ would have a saddle point instead of a maximum at $\mathbf{q}_c$). From Eq. (3.11) one sees that, as a consequence, the ellipses traced out by the level lines of $R_0(\mathbf{q})=R$ (or equivalently, $\sigma=0$) in the (q,p) plane, with R slightly above R_c, are very eccentric throughout the whole oblique-roll range. The long axis, corresponding to a short coherence length in

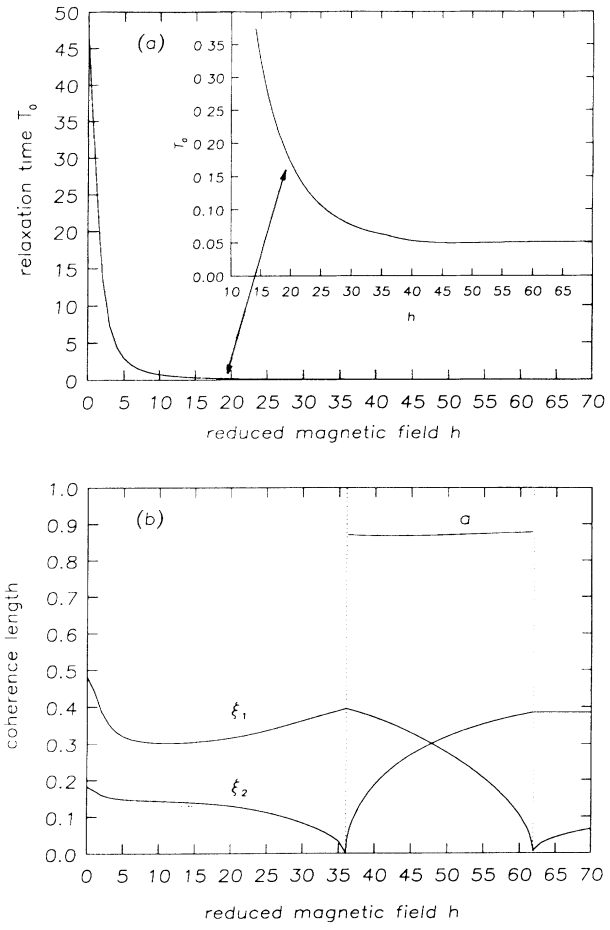

FIG. 3. (a) The relaxation time T_0, measured in units of the heat-diffusion time $d^2/\kappa_\perp$, as a function of the reduced magnetic field h. (b) The coherence lengths ξ_1,ξ_2, in units of the cell thickness d, and the cross coefficient a as function of h.

that direction, remains always roughly parallel to the rolls.

Instead of giving the nonlinear coefficient g which is usually defined with respect to a mathematically convenient normalization of the linear eigenvector, we have given in Sec. IV B some experimentally more relevant quantities. The quantity g has been calculated before [22,23] for $h=0$. It was positive indicating a forward bifurcation. A quantitative comparison is not possible because the normalization of the linear eigenvector was not given there.

Besides the simplified description of roll solutions and their stability, the amplitude equation allows one to describe many other properties, such as the structure and dynamics of defects [45] and of wavelength-changing processes [46]. For that purpose it is useful to realize that by appropriate scaling all parameters can be eliminated from Eq. (5.2). Therefore all pattern-forming instabilities with a steady forward bifurcation and axial anisotropy obey a simple law of similarity slightly above threshold.

VI. STABILITY OF ROLLS AT HIGHER ORDER

A. General formulation

In this section we describe the effects of higher-order terms in ϵ which are not contained in the amplitude-equation formalism in Sec. V. An important reason for going to second order in the amplitude [or $O(\epsilon)$] is that new destabilization mechanisms come in which may lead to spatiotemporal chaos. The new modes are characterized by spatial variations on a length scale much larger than that of the underlying roll pattern and develop continuously out of the $\mathbf{q}=0$ part of $\mathbf{V}_2$ (see Sec. IV A). The physical origin lies in the fact that bending of rolls induces pressure gradients which excite the so-called *mean flow* (or "large-scale" flow or "mean drift") with nonzero average over the cell height (it vanishes for straight rolls). Such a flow is also characterized by a nonvanishing vertical vorticity. In order to include mean-flow effects in the amplitude-equation formalism, one has to add an equation for the vertical vorticity. This has been done for isotropic systems first for free boundary conditions [47]. The equations were qualitatively correct but the results did not agree with a rigorous stability analysis of the full equations [48] and a further extension was necessary [39]. For rigid boundaries a corresponding equation has been given quite recently, but a comparison with rigorous results has not been performed [49]. The free-boundary case was recently discussed for EHC and spatiotemporal chaos was shown to occur then already at threshold for MBBA-like materials [50].

If one is interested only in the linear stability of rolls one can avoid amplitude equations, which are confined to long-wavelength scenarios and whose construction in our complicated system to order ϵ is not straightforward. It is then much simpler to stay in q space, as will be done in the following. The stability analysis is performed by writing

$$A(\mathbf{q},t)=A_r(\mathbf{q})+\delta A(\mathbf{q},t) , \tag{6.1}$$

where $A_r(\mathbf{q})$ was determined in Sec. IV, Eq. (4.3a), and

$$\delta A(\mathbf{q},t)=s_1(t)\delta(\mathbf{q}-\mathbf{q}_0-\alpha)+s_2(t)\delta(\mathbf{q}+\mathbf{q}_0-\alpha) , \tag{6.2}$$

with the modulation wave vector $\alpha=(\alpha_x,\alpha_y)$. Equation (6.1) gives rise to a perturbation $\delta\mathbf{V}_1$ of the lowest-order stationary-roll solution $\mathbf{V}_{1r}$ [for $\mathbf{V}_{1r}$ see (4.3a)]

$$\delta\mathbf{V}_1=s_1(t)\mathbf{V}_0(\mathbf{q}_0+\alpha)e^{i(\mathbf{q}_0+\alpha)\cdot\mathbf{x}} +s_2(t)\mathbf{V}_0(-\mathbf{q}_0+\alpha)e^{i(-\mathbf{q}_0+\alpha)\cdot x}+\text{c.c.} \tag{6.3}$$

Only contributions linear in s_1 and s_2 will be retained. The restriction to one wave vector α is sufficient because the equations close, and the most general disturbance can be constructed by superposition. From the second-order equation (4.4a) one sees that the corresponding perturbations $\delta\mathbf{V}_2$ of $\mathbf{V}_{2r}$ have wave vectors $\mathbf{q}=\alpha$, $\pm2\mathbf{q}_0+\alpha$ (those components of $\delta\mathbf{V}_2$ which correspond to the velocity potentials f and g with wave vector $\mathbf{q}=\alpha$ and $|\alpha|$ small, represent the mean-flow disturbances). At third order the equations are closed as usual by projecting Eq. (2.18) (linearized with respect to $\delta\mathbf{V}_1$ and $\delta\mathbf{V}_2$) onto the linear eigenvectors $\mathbf{V}(\mathbf{q}_0+\alpha)$ and $\mathbf{V}(-\mathbf{q}_0+\alpha)$. The time dependence of $s_1(t)$, $s_2(t)$, and $\delta\mathbf{V}_2$ are chosen proportional to $\exp(\lambda t)$ and then we obtain a linear problem to be solved for the eigenvalue λ. Some details of the derivation are sketched in Appendix C. If there exist $\alpha=(\alpha_x,\alpha_y)$ such that $\mathrm{Re}[\lambda(\mathbf{q},\epsilon;\alpha)]>0$, the stationary solution at $(\mathbf{q},\epsilon)$ is unstable; otherwise, it will be regarded as stable. A simplification is suggested by noting that $\lambda=0(\epsilon)$ [or $O(|s(\mathbf{q}_0)|^2)$] is consistent with the equations for $\delta\mathbf{V}_1$ [Eqs. (C11) and (C12)]. Then the time derivatives are of higher order in the equations for the second-order perturbation $\delta\mathbf{V}_2$ [Eqs. (C8)–(C10)] and can be neglected there. We have checked the validity of this approximation by comparison with the full numerical solution. With this adiabatic approximation $\delta\mathbf{V}_2$ is easily obtained as functions of s_1 and s_2 by solving a linear system in Fourier space leading to a 2×2 eigenvalue problem for λ. We have also tested that it is sufficient to keep in the third-order equation only the leading-time derivative which contains the operator B_0 [see Eq. (2.18)].

For normal rolls we use the standard definitions of the three long-wavelength instabilities ($\alpha_x,\alpha_y\to0$) which depend on the sequence of the limits: namely *Eckhaus instability* if $\alpha_y=0$, *zigzag instability* if $\alpha_x=0$, and *skewed-varicose instability* if α_x/α_y is finite. We have also found a short-wavelength instability for oblique rolls (see below).

The Eckhaus instability corresponds to local dilation and compression of the roll pattern; the zigzag instability leads to an undulation along the roll axis. These two instabilities are ubiquitous in pattern-forming systems and are well known also in isotropic systems. The skewed-varicose instability appears only if the contribution to the velocity in $\delta\mathbf{V}_2(\alpha)$ in second order is kept. The state the system evolves to cannot be obtained unambiguously from the linear perturbation analysis. Beyond the zigzag instability it could be an undulated roll pattern, oblique rolls, or possibly something else. As for the skewed-varicose instability there is evidence from numerical

simulations that a complicated dynamical state (defect turbulence) appears [5,7,50,51].

B. Results and discussion

In the following we describe some of the results of the stability analysis, which we consider to be the most interesting part of this work. We are mainly interested in the low-field region and in the behavior near the lower Lifshitz point, where we expect some analogies with EHC.

First we discuss the stability diagram in the normal-roll ($p=0$), forward-bifurcation range ($h<4.15$). In Fig. 4 the stable normal-roll region is shown in the ϵ-q plane for zero field (inside of the region limited by the dashed and upper solid curves). Also shown are the neutral curve (solid curve marked by NC) and the lowest-order Eckhaus parabola (dotted), which is the only stability limit obtained from the lowest-order analysis (amplitude equation). Figure 4 demonstrates the importance of the $O(\epsilon)$ contributions. On the solid curve marked by E destabilization occurs by the Eckhaus mechanism, i.e., with the modulation wave vector parallel to q. Compared to the lowest-order result there is an asymmetry to the left. It is interesting to note that this asymmetry is opposite to that of the neutral curve. On the dashed curve one has a skewed-varicose (SV) instability, i.e., the modulation wave vector is oblique and mean flow is decisive. The stability curves (E and SV) reach the neutral curve at the point P (wave number $q=q_P$). We found that for $q<q_P$ $c_3(q)$ is positive [see (4.6)], therefore on the neutral curve the bifurcation type changes (forward $\leftrightarrow$ backward) at P so that this point could be called a "tricritical point in the ϵ-q plane." This scenario can be described by introducing spatial derivatives into the nonlinear term in the conventional amplitude equation and one can show indeed that the Eckhaus stability curve approaches the neutral surface at P (the details will be published elsewhere). For increasing magnetic field P comes down along the neutral curve and crosses the point $q=q_c$ at $h=4.15$. In Fig. 5 the onset of the SV instability at band center, i.e., for $q=q_c$, is plotted as a function of h. The stability limit reduces to $\epsilon=0$ as the tricritical point P coincides with the threshold.

In order to explore the possible transitions when the SV limit is reached for increasing ϵ, we have examined the stability of rolls with $p\neq 0$ at $h=0$. For given q we find that the stability limit ϵ decreases for increasing p. Therefore a transition to oblique rolls is excluded. There remains the possibility of a transition to a more complicated spatial structure, or possibly, spatiotemporal chaos.

In the high-field, normal-roll, forward-bifurcation region ($31<h<36$) the situation is different. In Fig. 6 the neutral curve and the various instabilities are shown in the ϵ-q plane for $h=34$, slightly below the lower Lifshitz point ($h=36$) at which the transition between normal and oblique rolls occurs. The Eckhaus instability is now asymmetric to the right, like the neutral curve. The stable region is limited from above by a zigzag (or undulatory) instability (dashed) with a modulation wave vector perpendicular to q, which is expected to lead to oblique rolls. The zigzag curve meets the neutral curve at the point L where $q=q_L$. Our numerical calculations show that for $q>q_L$ one has $\partial^2 R_0/\partial^2 p>0$ while $\partial^2 R_0/\partial^2 p<0$ for $q<q_L$, so that for $q<q_L$ oblique rolls have a lower onset than normal rolls and L is therefore a "Lifshitz point in the ϵ-q plane." When the actual normal-oblique transition at $h=36$ is approached the point L moves down along the neutral curve and reaches $q=q_c$. One also sees from Fig. 6 that in some range of ϵ the right Eckhaus limit is preceded by a SV instability. The point P marks again the "tricritical point in the ϵ-q plane": $c_3(q)$ becomes positive for $q>q_P$.

In order to verify that at the zigzag instability a transition to oblique rolls is possible we have again extended the stability analysis to oblique rolls. Figure 7 shows the

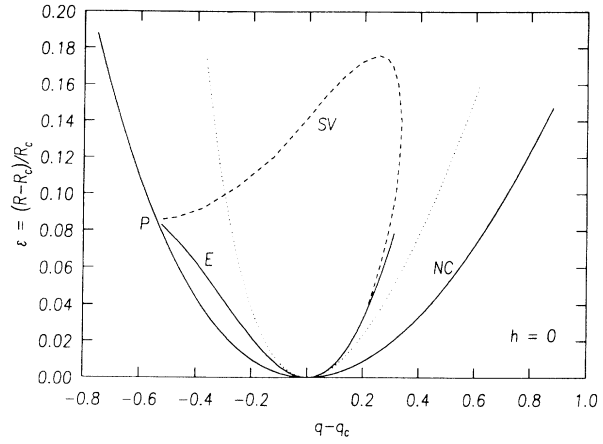

FIG. 4. Stability diagram for $h=0$ in the ϵ-q plane ($p=p_c=0$). NC; neutral curve. Dotted line: lowest-order Eckhaus parabola. E: calculated Eckhaus stability borderline. SV: skewed-varicose stability limit. The Eckhaus and SV lines merge at the "tricritical point" P. Rolls are stable inside the region bounded by the E and SV lines.

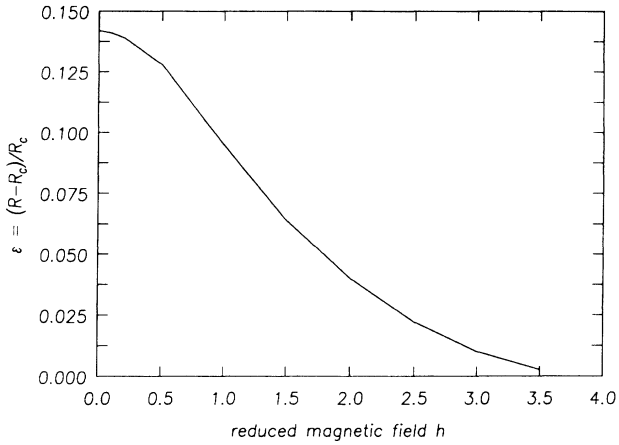

FIG. 5. Onset of the SV instability at the band center ($\mathbf{q}=\mathbf{q}_c$) as a function of h. The stability region shrinks to zero at the onset of the subcritical bifurcation.

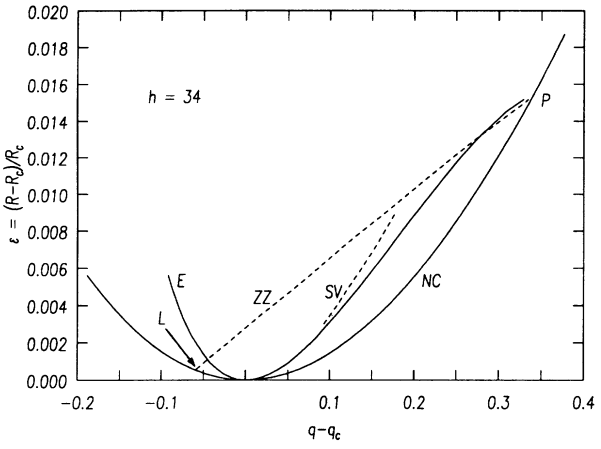

FIG. 6. Stability diagram for $h=34$ in the ϵ-q plane ($p=p_c=0$). The stability region is now bounded from above by the zigzag (ZZ) instability (pure undulations along the rolls), which emanates from the Lifshitz-point L on the neutral curve.

results in the ϵ-p plane at fixed $q=q_c$ for the same field $h=34$. The neutral curve and the Eckhaus limit are as expected. The extension of the zigzag instability to finite p (dashed) is curved upward, so that oblique rolls indeed remain stable after the normal rolls have lost stability. Eventually, at larger ϵ, we find that oblique rolls become unstable (dotted lines) with respect to disturbances with nonzero modulation wave vectors α_y. Such short-wavelength instabilities could maybe lead to the development of oblique rolls with the wave vector around $(q_c,-p)$. The scenario would then have some similarity to the cross-roll instability [42] in isotropic fluids. In both cases the roll pattern becomes unstable to modes which correspond to an equivalent degenerate configuration. Beyond the stability limit one could have a dynamic situation

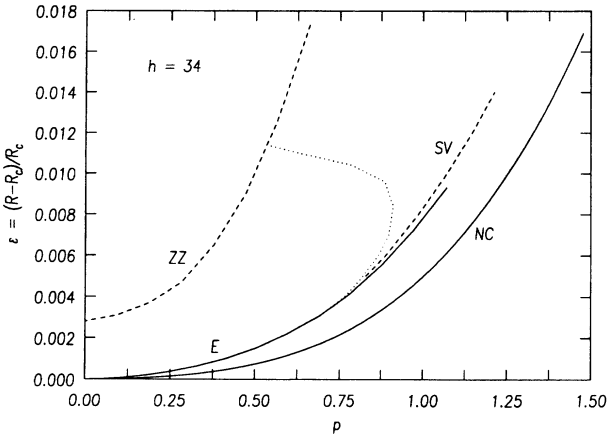

FIG. 7. Stability diagram for $h=34$ in the ϵ-p plane at q_c. The stable region is bounded by the E, SV, and ZZ lines and in addition by the dotted line, at which a short-wavelength destabilization sets in. The curves continue symmetrically to $p<0$.

characterized by oscillations between two degenerate oblique rolls (a bimodal, rectangular structure is also possible). In the magnetic-field range where oblique rolls occur at threshold we have only convinced ourselves that rolls with critical wave vector $\mathbf{q}_c$ are stable immediately above onset.

VII. CONCLUDING REMARKS

We hope that our predictions stimulate new experiments. In fact, in preliminary measurements on 5CB (planar configuration) backward bifurcations have been observed in the intermediate magnetic-field range [52]. The parameters of the amplitude equation and the stability regions may be measured by methods introduced for EHC [10,14,15].

We have not been able to determine the state which the system evolves to once all roll solutions have become unstable. In order to do this one would have to test more complicated (bimodal) patterns for stability. These patterns include undulated normal and oblique rolls as observed in EHC (the latter can presumably be identified with the "skewed-varicose" pattern observed sometimes [8], and were shown to exist in the vicinity of the normal-oblique transition [31,46]). Moreover, one would have to construct a generalized amplitude equation including mean-flow in order to test transitions to spatiotemporal chaos. For EHC with free boundary conditions this has been done, and for MBBA-like materials one always finds spatiotemporal chaos [46,50]. Subsequently amplitude equations were constructed on a phenomenological basis and used to investigate the various instabilities [51]. A simulation with a coupled-map-lattice approach was also performed there and apparently the defect-mediated turbulence was obtained [51].

Comparing our results with those found in EHC within the standard theory [13,53] we note that one of the essential differences is the absence of a backward bifurcation in the latter case. Also in EHC the destabilization of the primary normal-roll structure appears to occur always by the zigzag scenario, similar to RBC in nematics in the high-field case.

We point out that an investigation similar to the one presented here is underway for RBC in nematic liquid crystals with homeotropic alignment. This very rich system [19,54,55] has two main distinguishing features: Without additional magnetic field it is isotropic in the plane of the layer and thus shares many properties with RBC in simple fluids. By adding a horizontal magnetic field an anisotropy can be turned on continuously. Second, a Hopf bifurcation leading to a time-periodic convection pattern can occur [28,29,54].

ACKNOWLEDGMENTS

We wish to thank W. Decker, M. Kaiser, and W. Zimmermann for useful discussions and help in the programming, as well as G. Ahlers and L. I. Berge for communicating to us their early experimental results. Financial support by Deutsche Forschungsgemeinschaft (SFB 213, Bayreuth) and Fonds der Chemischen Industrie is gratefully acknowledged.

APPENDIX A

We have measured lengths in units of d (slab thickness) and the time in units of the heat-diffusion time $d^2/\kappa_\perp$. The temperature scaling follows the convention used in isotropic RB convection: $\phi=\phi'[(\alpha_4/2)\kappa_\perp/(\alpha g d^3\rho_0)]$. The viscosity coefficients, elastic constants, and heat diffusivities are scaled as $\alpha_i=\alpha_i'(\alpha_4/2)$, $k_{ii}=k_{ii}'k_{ii}$, $\kappa_\parallel=\kappa_\parallel'\kappa_\perp$, $\kappa_a=\kappa_a'\kappa_\perp$. The other dimensionless quantities are defined in Eqs. (2.16) and (2.17). After dropping the primes the equations for the temperature, director, and velocity read in dimensionless form (coordinates defined in Sec. II)

$$-\frac{d\phi}{dt}+\partial_1[\kappa_a n_i n_j(\partial_j\phi-R\delta_{j3})+\partial_i\phi]+Rv_z=0\ , \tag{A1}$$

$$(1-n_z^2)\Gamma_z-n_x n_z\Gamma_x-n_y n_z\Gamma_y=0\ , \tag{A2}$$

$$-n_x\Gamma_y+n_y\Gamma_x=0\ , \tag{A3}$$

$$\delta_i\left[-(1/P_r)\frac{dv_i}{dt}+\phi\delta_{i3}+\partial_j(s_{ji}\gamma_1/F+t_{ji})\right]=0\ , \tag{A4}$$

$$\epsilon_i\left[-(1/P_r)\frac{dv_i}{dt}+\phi\delta_{i3}+\partial_j(s_{ji}\gamma_1/F+t_{ji})\right]=0\ . \tag{A5}$$

In (A4) and (A5) the operators $\delta=(\partial_x\partial_z,\partial_y\partial_z,-\partial_x^2-\partial_y^2)$ and $\epsilon=(\partial_y,-\partial_x,0)$ have been applied to eliminate the pressure. $\mathbf{\Gamma}$ is given by

$$\mathbf{\Gamma}=-\frac{\delta G}{\delta\mathbf{n}}-F\mathbf{N}-F(\gamma_2/\gamma_1)\mathbf{A}\cdot\mathbf{n}+\pi^2(\mathbf{n}\cdot\mathbf{h})\mathbf{h}\ . \tag{A6}$$

The expressions for quantities G, $\mathbf{N}$, and $\mathbf{A}$ in (A6) and t_{ij},s_{ij} in (A4) and (A5) are the same as those given in Sec. II with the material parameters replaced by dimensionless ones. Finally the system (A1)–(A5) is expanded with respect to ϕ, n_z, n_y, f, and g and can be written in the form of (2.18).

APPENDIX B

Our results have been obtained with the following material parameters for the nematic liquid crystal MBBA [30]:

$$(k_{11},k_{22},k_{33})=(6\times10^{-12}\ \mathrm{N},4\times10^{-12}\ \mathrm{N},7\times10^{-12}\ \mathrm{N})\ ,$$

$$(\alpha_1,\alpha_2,\alpha_3,\alpha_4,\alpha_5,\alpha_6)=(6.5\times10^{-3}\ \mathrm{kg\,m^{-1},s^{-1}}-77.5\times10^{-3}\ \mathrm{kg\,m^{-1}\,s^{-1}},$$
$$-1.2\times10^{-3}\ \mathrm{kg\,m^{-1}\,s^{-1}},83.2\times10^{-3}\ \mathrm{kg\,m^{-1}\,s^{-1}}\ ,$$
$$46.3\times10^{-3}\ \mathrm{kg\,m^{-1}\,s^{-1}},-32.4\times10^{-3}\ \mathrm{kg\,m^{-1}\,s^{-1}})\ ,$$

$$(\kappa_\parallel,\kappa_\perp)=(1.54\times10^{-7}\ \mathrm{m^2\,s^{-1}},0.93\times10^{-7}\ \mathrm{m^2\,s^{-1}}),\ \rho_0=1000\ \mathrm{kg\,m^{-3}}\ .$$

The Prandtl number and the relaxation time ratio are $P_r=447.31$ and $F=1182.65$, respectively. For two typical values of the thickness, $d=1$ and 5 mm, the Fréedericksz transition thresholds H_f are 69.39 and 13.88 G, respectively ($\chi_a=1.23\times10^{-7}$ in cgs units).

APPENDIX C

In the following we present in more detail the method for the stability analysis sketched in Sec. VI A. Substituting (6.1) and (6.2) into (4.2) gives a leading-order ansatz for the time-dependent solution $\mathbf{V}_1$, which is a superposition of the stationary solution $\mathbf{V}_{1r}$ and the perturbation $\delta\mathbf{V}_1$

$$\mathbf{V}_1=\mathbf{V}_{1r}+\delta\mathbf{V}_1\ , \tag{C1}$$

with

$$\mathbf{V}_{1r}=s(\mathbf{q})\mathbf{V}_0(\mathbf{q})e^{i\mathbf{q}\cdot\mathbf{x}}+\text{c.c.}\equiv\mathbf{v}_1e^{i\mathbf{q}\cdot\mathbf{x}}+\text{c.c.}\ , \tag{C2}$$

$$\delta\mathbf{V}=e^{\lambda t}[s_1\mathbf{V}_0(\mathbf{q}+\alpha)e^{i(\mathbf{q}+\alpha)\cdot\mathbf{x}}$$
$$+s_2\mathbf{V}_0(-\mathbf{q}+\alpha)e^{i(-\mathbf{q}+\alpha)\cdot\mathbf{x}}]\ . \tag{C3}$$

In (C2) the shorthand notation $\mathbf{v}_1\equiv s(\mathbf{q})\mathbf{V}_0(\mathbf{q})$ has been introduced.

In second order $\delta\mathbf{V}_1$ will lead to a disturbance $\delta\mathbf{V}_2$ of the stationary part $\mathbf{V}_{2r}$

$$\mathbf{V}_2=\mathbf{V}_{2r}+\delta\mathbf{V}_2\ . \tag{C4}$$

$\mathbf{V}_{2r}$ is determined from Eq. (4.4a) and can be written in the form

$$\mathbf{V}_{2r}\equiv\mathbf{v}_2(2\mathbf{q})e^{2i\mathbf{q}\cdot\mathbf{x}}+\mathbf{v}_2(-2\mathbf{q})e^{-2i\mathbf{q}\cdot\mathbf{x}}+\mathbf{v}_2(0)\ . \tag{C5}$$

The time dependence of $\mathbf{V}_2$ is governed by [see Eq. (2.18)]

$$B_0\partial_t\mathbf{V}_2=L\mathbf{V}_2+\mathbf{N}_2(\mathbf{V}_1|\mathbf{V}_1)\ , \tag{C6}$$

where the term $B_1(\mathbf{V}_1)\partial_t\mathbf{V}_1$ has been incorporated into $\mathbf{N}_2(\mathbf{V}_1|\mathbf{V}_1)$ without changing the notation. $\delta\mathbf{V}_2$ can be expressed as

$$\delta\mathbf{V}_2=e^{\lambda t}(T_+e^{i(2\mathbf{q}+\alpha)\cdot\mathbf{x}}+T_-e^{i(-2\mathbf{q}+\alpha)\cdot\mathbf{x}}+T_0e^{i\alpha\cdot\mathbf{x}})\ , \tag{C7}$$

with the unknowns T_+, T_-, and T_0 whose z dependence has the same symmetry as $\mathbf{V}_{2r}$ and is treated by the same Galerkin expansion.

Now substituting $\mathbf{V}_1=\mathbf{V}_{1r}+\delta\mathbf{V}_1$ and $\mathbf{V}_2=\mathbf{V}_{2r}+\delta\mathbf{V}_2$ into (C6) and linearizing with respect to $\delta\mathbf{V}_1$ and $\delta\mathbf{V}_2$, one obtains

$$\lambda B_0\mathbf{T}_+=L\mathbf{T}_++\{\mathbf{N}_2[\mathbf{v}_1|\mathbf{V}_0(+)]+\mathbf{N}_2[\mathbf{V}_0(+)|\mathbf{v}_1]\}s_1\ , \tag{C8}$$

$$\lambda B_0 \mathbf{T}_- = L\mathbf{T}_- + \{\mathbf{N}_2[\mathbf{v}_1^*|\mathbf{V}_0(-)] + \mathbf{N}_2[\mathbf{V}_0(-)|\mathbf{v}_1^*]\}s_2 \ , \tag{C9}$$

$$\lambda B_0 \mathbf{T}_0 = L\mathbf{T}_0 + \{\mathbf{N}_2[\mathbf{v}_1^*|\mathbf{V}_0(+)] + \mathbf{N}_2[\mathbf{V}_0(+)|\mathbf{v}_1^*]\}s_1 + \{\mathbf{N}_2[\mathbf{v}_1|\mathbf{V}_0(-)] + \mathbf{N}_2[\mathbf{V}_0(-)|\mathbf{v}_1]\}s_2 \ . \tag{C10}$$

In (C8)–(C10) the abbreviation $\mathbf{V}_0(\pm) := \mathbf{V}_0(\pm\mathbf{q}+\alpha)$ has been used, and all operators (B_0, L, $\mathbf{N}_2$, and $\mathbf{N}_3$) are understood to act in Fourier space. We then insert $\mathbf{V} = \mathbf{V}_1 + \mathbf{V}_2$ into (2.18) and linearize it. After taking scalar products [see Eq. (3.10)] with $\mathbf{U}(\mathbf{q}+\alpha)$ and $\mathbf{U}(-\mathbf{q}+\alpha)$, eigenvectors adjoint to $\mathbf{V}_0(\mathbf{q}+\alpha)$ and $\mathbf{V}_0(-\mathbf{q}+\alpha)$, respectively, we find

$$\begin{aligned}\lambda\langle \mathbf{U}(\mathbf{q}+\alpha), B_0\mathbf{V}_0(+)\rangle s_1 = {} & \langle \mathbf{U}(\mathbf{q}+\alpha), L\mathbf{V}_0(+)\rangle s_1 + \langle \mathbf{U}(\mathbf{q}+\alpha), \mathbf{N}_2(\mathbf{v}_1^*|T_+) + \mathbf{N}_2(\mathbf{T}_+|\mathbf{v}_1^*) + \mathbf{N}_2(\mathbf{v}_1|\mathbf{T}_0) + \mathbf{N}_2(\mathbf{T}_0|\mathbf{v}_1)\rangle \\ & + \langle \mathbf{U}(\mathbf{q}+\alpha), \{\mathbf{N}_2[\mathbf{V}_0(+)|\mathbf{v}_2(0)] + \mathbf{N}_2[\mathbf{v}_2(0)|\mathbf{V}_0(+)] \\ & \quad + N_3[\mathbf{v}_1|\mathbf{v}_1^*|\mathbf{V}_0(+)] + \mathbf{N}_3[\mathbf{v}_1|\mathbf{V}_0(+)|\mathbf{v}_1^*] + \mathbf{N}_3[\mathbf{V}_0(+)|\mathbf{v}_1|\mathbf{v}_1^*] \\ & \quad + \mathbf{N}_3[\mathbf{v}_1^*|\mathbf{v}_1|\mathbf{V}_0(+)] + \mathbf{N}_3[\mathbf{v}_1^*|\mathbf{V}_0(+)|\mathbf{v}_1] + \mathbf{N}_3[\mathbf{V}_0(+)|\mathbf{v}_1^*|\mathbf{v}_1]\}\rangle s_1 \\ & + \langle \mathbf{U}(\mathbf{q}+\alpha), \{\mathbf{N}_2[\mathbf{V}_0(-)|\mathbf{v}_2(2\mathbf{q})] + \mathbf{N}_2[\mathbf{v}_2(2\mathbf{q})|\mathbf{V}_0(-)] \\ & \quad + \mathbf{N}_3[\mathbf{v}_1|\mathbf{v}_1|\mathbf{V}_0(-)] + \mathbf{N}_3[\mathbf{v}_1|\mathbf{V}_0(-)|\mathbf{v}_1] + \mathbf{N}_3[\mathbf{V}_0(-)|\mathbf{v}_1|\mathbf{v}_1]\}\rangle s_2 \ ,\end{aligned} \tag{C11}$$

$$\begin{aligned}\lambda\langle \mathbf{U}(-\mathbf{q}+\alpha), B_0\mathbf{V}_0(-)\rangle s_2 = {} & \langle \mathbf{U}(-\mathbf{q}+\alpha), L\mathbf{V}_0(-)\rangle s_2 \\ & + \langle \mathbf{U}(-\mathbf{q}+\alpha), \mathbf{N}_2(\mathbf{v}_1|T_-) + \mathbf{N}_2(\mathbf{T}_-|\mathbf{v}_1) + \mathbf{N}_2(\mathbf{v}_1^*|T_0) + \mathbf{N}_2(\mathbf{T}_0|\mathbf{v}_1^*)\rangle \\ & + \langle \mathbf{U}(-\mathbf{q}+\alpha), \{\mathbf{N}_2[\mathbf{V}_0(+)|\mathbf{v}_2(-2\mathbf{q})] + \mathbf{N}_2[\mathbf{v}_2(-2\mathbf{q})|\mathbf{V}_0(+)] \\ & \quad + \mathbf{N}_3[\mathbf{v}_1^*|\mathbf{v}_1^*|\mathbf{V}_0(+)] + \mathbf{N}_3[\mathbf{v}_1^*|\mathbf{V}_0(+)|\mathbf{v}_1^*] + \mathbf{N}_3[\mathbf{V}_0(+)|\mathbf{v}_1^*|\mathbf{v}_1^*]\}\rangle s_1 \\ & + \langle \mathbf{U}(-\mathbf{q}+\alpha), \{\mathbf{N}_2[\mathbf{V}_0(-)|\mathbf{v}_2(0)] + \mathbf{N}_2[\mathbf{v}_2(0)|\mathbf{V}_0(-)] \\ & \quad + \mathbf{N}_3[\mathbf{v}_1|\mathbf{v}_1^*|\mathbf{V}_0(-)] + \mathbf{N}_3[\mathbf{v}_1|\mathbf{V}_0(-)|\mathbf{v}_1^*] + \mathbf{N}_3[\mathbf{V}_0(-)|\mathbf{v}_1|\mathbf{v}_1^*] \\ & \quad + \mathbf{N}_3[\mathbf{v}_1^*|v_1|V_0(-)] + \mathbf{N}_3[\mathbf{v}_1^*|\mathbf{V}_0(-)|\mathbf{v}_1] + \mathbf{N}_3[\mathbf{V}_0(-)|\mathbf{v}_1^*|\mathbf{v}_1]\}\rangle s_2 \ .\end{aligned} \tag{C12}$$

Equations (C8)–(C12) are solved numerically for the eigenvalue $\lambda(\mathbf{q}, \epsilon; \alpha)$. Positive $\mathrm{Re}(\lambda)$ signals instability.

[1] F. H. Busse, Rep. Prog. Phys. **41**, 28 (1978); in *Hydrodynamic Instabilities and the Transition to Turbulence,* 2nd ed., edited by H. L. Swinney and J. P. Gollub (Springer, Berlin, 1986); in *Mantle Convectiom, Plate Tectonics and Global Dynamics,* edited by W. R. Peltier (Gordon and Breach, New York, 1989).

[2] M. S. Heutmaker, P. N. Fraenkel, and J. P. Gollub, Phys. Rev. Lett. **54**, 1369 (1985); G. Ahlers, D. S. Cannell, and V. Steinberg, *ibid.* **54**, 1373 (1985); P. Le Gal, A. Pocheau, and V. Croquette, *ibid.* **54**, 2501 (1985); **55**, 1094 (1985).

[3] E. Moses, J. Fineberg, and V. Steinberg, Phys. Rev. A **35**, 2757 (1987); R. Heinrichs, G. Ahlers, and D. S. Cannell, *ibid.* **35**, 2761 (1987); P. Kolodner, D. Bensimon, and C. M. Surko, Phys. Rev. Lett. **60**, 1723 (1988).

[4] W. Eckhaus, *Studies in Nonlinear Stability Theory* (Springer, New York, 1965); L. Kramer and W. Zimmermann, Physica D **16**, 221 (1985).

[5] See, e.g., P. Manneville, *Dissipative Structures and Weak Turbulence* (Academic, New York, 1990).

[6] R. M. Clever and F. H. Busse, J. Appl. Math. Phys. **29**, 711 (1978); F. H. Busse and R. M. Clever, J. Fluid. Mech. **91**, 319 (1979).

[7] F. H. Busse, Contemp. Math. **56**, 1 (1986); H. S. Greenside, W. M. Coughran, and N. L. Schryer, Phys. Rev. Lett. **49**, 726 (1982).

[8] A. Joets and R. Ribotta, in *Cellular Structure in Instabilities,* edited by J. E. Wesfreid and S. Zaleski (Springer, Berlin, 1984); J. Phys. (Paris) **47**, 595 (1986); R. Ribotta, A. Joets, and Lin Lei, Phys. Rev. Lett. **56**, 1595 (1986).

[9] S. Kai and W. Zimmermann, Prog. Theor. Phys. Suppl. **99**, 458 (1989).

[10] S. Rasenat, V. Steinberg, and I. Rehberg, Phys. Rev. A **42**, 5998 (1990).

[11] E. Bodenschatz, W. Zimmermann, and L. Kramer, J. Phys. (Paris) **49**, 1875 (1988).

[12] L. Kramer, E. Bodenschatz, W. Pesch, W. Thom, and W. Zimmermann, Liq. Cryst. **5**, 699 (1989).

[13] W. Pesch, W. Decker, Q. Feng, M. Kaiser, L. Kramer, and A. Weber, in *Defects, Singularities and Patterns in Nematic Liquid Crystals,* Vol. 332 of *NATO Advanced Study Institute, Series C: Mathematical and Physical Sciences,* edited by J. M. Coron, F. Helein, and J.M. Ghidaglia (Kluwer, Amsterdam, 1991).

[14] S. Nasuno and S. Kai, Europhys. Lett. **14**, 779 (1991).

[15] E. Braun, and S. Rasenat, and V. Steinberg, Europhys. Lett. **15**, 597 (1991).
[16] E. Dubois-Violette, C. R. Acad. Sci. **21**, 923 (1971).
[17] E. Dubois-Violette, E. Guyon, and P. Pieranski, Mol. Cryst. Liq. Cryst. **26**, 193 (1974).
[18] E. Dubois-Violette, G. Durand, E. Guyon, P. Manneville, and P. Pieranski, *Solid State Physics,* edited by L. Liebert (Academic, New York, 1978), Suppl. 14.
[19] See P. J. Barratt, Liq. Cryst. **4**, 223 (1989), and the references therein.
[20] W. Zimmermann, Ph.D. thesis, University of Bayreuth, 1988 (unpublished).
[21] A. Joets, L. Kramer, R. Ribotta, and W. Zimmermann (unpublished).
[22] E. Dubois-Violette and F. Rothen, J. Phys. (Paris) **40**, 1013 (1979).
[23] D. A. Hodson, P. J. Barratt, and D. M. Sloan, J. Non-Equilib. Thermodyn. **9**, 107 (1984).
[24] P. G. de Gennes, *The Physics of Liquid Crystals* (Clarendon, Oxford, 1974); S. Chandrasekhar, *Liquid Crystals* (Cambridge University, Cambridge, England, 1977); M. J. Stephen and J. P. Straley, Rev. Mod. Phys. **46**, 617 (1974).
[25] F. H. Busse, J. Fluid. Mech. **52**, 97 (1972).
[26] R. M. Clever and F.H. Busse, J. Fluid Mech., **65**, 625 (1974).
[27] S. Chandrasekhar, *Hydrodynamic and Hydromagnetic Stability* (Clarendon, Oxford, 1961).
[28] H. N. W. Lekkerkerker, J. Phys. (Paris) **38**, L-277 (1977).
[29] E. Dubois-Violette and M. Gabay, J. Phys. (Paris) **43**, 1305 (1982).
[30] P. J. Barratt and D. M. Sloan, J. Phys. A **9**, 1987 (1976).
[31] W. Pesch and L. Kramer, Z. Phys. B **63**, 121 (1986).
[32] C. Fraser, Mol. Cryst. Liq. Cryst. **94**, 327 (1983); P. J. Barratt and I. Zuniga, J. Non-Equilib. Thermodyn. **10**, 233 (1985).
[33] E. Dubois-Violette, Solid State Commun. **14**, 767 (1974).
[34] M. G. Velarde and I. Zuniga, J. Phys. (Paris) **40**, 725 (1979).
[35] P. J. Barratt and J. M. Manley, J. Non-Equilib. Thermodyn. **8**, 143 (1983).
[36] J. Carr, *Applications of Center Manifold Theory,* Applied Mathematical Sciences Vol. 35 (Springer, Berlin, 1981).
[37] H. Haken, *Synergetics,* 2nd ed. (Springer-Verlag, Berin, 1978).
[38] M. C. Cross, Phys. Fluids **23**, 1727 (1980).
[39] A. J. Bernoff (unpublished).
[40] E. A. Spiegel, in Woods Hole Oceanographic Institute Technical Report No. WHOI-85-36, edited by G. Veronis and L. M. Hudon (unpublished).
[41] A. C. Newell and J. A. Whitehead, J. Fluid Mech. **38**, 279 (1969); L. A. Segel, *ibid.* **38**, 203 (1969).
[42] F. H. Busse, J. Math. Phys. **46**, 140 (1967).
[43] D. A. Hodson, P. J. Barratt, and D. M. Sloan, J. Non-Equilib. Thermodyn. **10**, 37 (1985).
[44] E. Bodenschatz, Ph.D. thesis, University of Bayreuth, 1989 (unpublished).
[45] E. Bodenschatz, W. Pesch, and L. Kramer, Physica D **32**, 135 (1988).
[46] E. Bodenschatz, M. Kaiser, L. Kramer, W. Pesch, A. Weber, and W. Zimmermann, in *New Trends in Nonlinear Dynamics and Pattern Forming Phenomena: The Geometry of Nonequilibrium, NATO Advanced Study Institute, Series B: Physics,* edited by P. Coullet and P. Huerre (Plenum, New York, 1989).
[47] A. Zippelius and E. Siggia, Phys. Fluids **26**, 2905 (1983).
[48] F. H. Busse and E. W. Bolton, J. Fluid Mech. **146**, 115 (1984).
[49] A. C. Newell, T. Passot, and M. Souli, J. Fluid. Mech. **220**, 187 (1990).
[50] M. Kaiser, W. Pesch, and E. Bodenschatz (unpublished).
[51] S. Sasa, Prog. Theor. Phys. **83**, 824 (1990); S. Sasa (unpublished).
[52] L. I. Berge, G. Ahlers, and D. S. Cannell (private communication).
[53] M. Kaiser, W. Decker, and W. Pesch (unpublished); W. Decker, Diploma thesis, Bayreuth, 1989 (unpublished).
[54] E. Guyon, P. Pieranski, and J. Salan, J. Fluid Mech. **93**, 65 (1979).
[55] J. Salan and E. Guyon, J. Fluid Mech. **126**, 13 (1983).